NASA/TP–2015–218575
An errata was added to this document, October 2016.

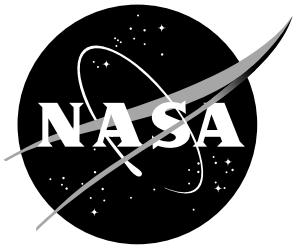

Battery-operated Independent Radiation Detector Data Report from Exploration Flight Test 1

Amir A. Bahadori, Edward J. Semones
NASA Johnson Space Center - Houston, Texas, USA

Ramona Gaza, Martin Kroupa, Ryan R. Rios, Nicholas N. Stoffle
Lockheed Martin Information Systems and Global Solutions - Houston, Texas, USA

Thomas Campbell-Ricketts, Lawrence S. Pinsky, Daniel Turecek
University of Houston - Houston, Texas, USA

June 2015

NASA STI Program . . . in Profile

Since its founding, NASA has been dedicated to the advancement of aeronautics and space science. The NASA scientific and technical information (STI) program plays a key part in helping NASA maintain this important role.

The NASA STI Program operates under the auspices of the Agency Chief Information Officer. It collects, organizes, provides for archiving, and disseminates NASA's STI. The NASA STI Program provides access to the NASA Aeronautics and Space Database and its public interface, the NASA Technical Report Server, thus providing one of the largest collection of aeronautical and space science STI in the world. Results are published in both non-NASA channels and by NASA in the NASA STI Report Series, which includes the following report types:

- TECHNICAL PUBLICATION. Reports of completed research or a major significant phase of research that present the results of NASA programs and include extensive data or theoretical analysis. Includes compilations of significant scientific and technical data and information deemed to be of continuing reference value. NASA counterpart of peer-reviewed formal professional papers, but having less stringent limitations on manuscript length and extent of graphic presentations.
- TECHNICAL MEMORANDUM. Scientific and technical findings that are preliminary or of specialized interest, e.g., quick release reports, working papers, and bibliographies that contain minimal annotation. Does not contain extensive analysis.
- CONTRACTOR REPORT. Scientific and technical findings by NASA-sponsored contractors and grantees.
- CONFERENCE PUBLICATION. Collected papers from scientific and technical conferences, symposia, seminars, or other meetings sponsored or co-sponsored by NASA.
- SPECIAL PUBLICATION. Scientific, technical, or historical information from NASA programs, projects, and missions, often concerned with subjects having substantial public interest.
- TECHNICAL TRANSLATION. English- language translations of foreign scientific and technical material pertinent to NASA's mission.

Specialized services also include organizing and publishing research results, distributing specialized research announcements and feeds, providing information desk and personal search support, and enabling data exchange services.

For more information about the NASA STI Program, see the following:

- Access the NASA STI program home page at ***http://www.sti.nasa.gov***
- E-mail your question to help@sti.nasa.gov
- Fax your question to the NASA STI Information Desk at 443-757-5803
- Phone the NASA STI Information Desk at 443-757-5802
- Write to:
  NASA STI Information Desk
  NASA Center for AeroSpace Information
  7115 Standard Drive
  Hanover, MD 21076–1320

NASA/TP–2015–218575
An errata was added to this document, October 2016.

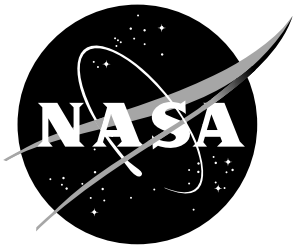

Battery-operated Independent Radiation Detector Data Report from Exploration Flight Test 1

Amir A. Bahadori, Edward J. Semones
NASA Johnson Space Center - Houston, Texas, USA

Ramona Gaza, Martin Kroupa, Ryan R. Rios, Nicholas N. Stoffle
Lockheed Martin Information Systems and Global Solutions - Houston, Texas, USA

Thomas Campbell-Ricketts, Lawrence S. Pinsky, Daniel Turecek
University of Houston - Houston, Texas, USA

National Aeronautics and
Space Administration

Johnson Space Center
Houston, Texas 77058

June 2015

Errata
Issued October 2016 for

NASA/TP-2015-218575

Battery-operated Independent Radiation Detector Data Report from Exploration Flight Test 1

Amir A. Bahadori, Edward J. Semones, Ramona Gaza, Martin Kroupa, Ryan R. Rios, Nicholas N. Stoffle, Thomas Campbell-Ricketts, Lawrence S. Pinsky, Daniel Turecek

Summary of Changes:

Section 4.6 (page 29):

Replace Figure 22 with the updated figure:

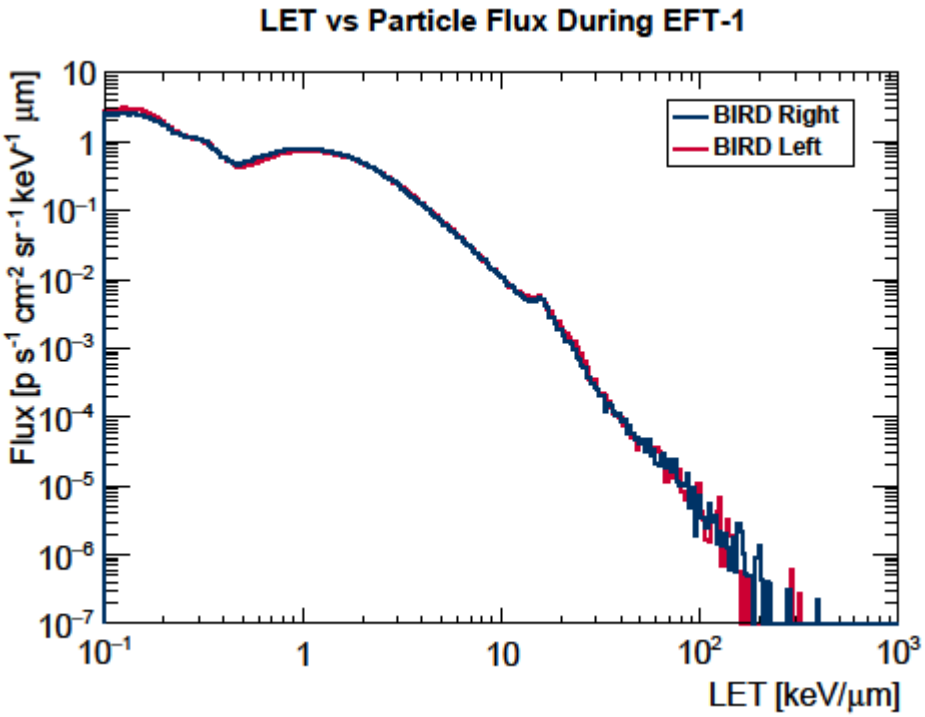

(This page intentionally left blank.)

Acknowledgments

The Battery-operated Independent Radiation Detector (BIRD) Science Team would like to acknowledge the entire BIRD team for contributing to a successful flight. Specifically, Madelyn Gruseck (BIRD Mechanical Engineer), Ronn Moore (BIRD Software Engineer), and Bobbie Gail Swan (Advanced Exploration Systems (AES) RadWorks Radiation Environment Monitor (REM) Project Manager) worked tirelessly during the Thanksgiving 2014 holiday to ensure that the BIRD was integrated properly in the Orion Multi-Purpose Crew Vehicle (MPCV) for Exploration Flight Test 1 (EFT-1). We would also like to thank Joe LeBlanc (Lockheed Martin) for supporting BIRD from its inception through the flight. Regina Senegal and Katie Nguyen (NASA Quality Assurance) helped tremendously with ensuring that the necessary paperwork was completed for shipping BIRD to and processing BIRD at Kennedy Space Center (KSC). We acknowledge the Medipix2 collaboration, based at the European Organization for Nuclear Research (CERN) for their assistance, and we thank Tim Sweet (NASA Engineering) for leading the design and testing of the BIRD hardware. We appreciate the creativity of Scott Black's pre-Advanced Placement physics class at Clear Falls High School in helping to name the BIRD. Finally, extensive testing of the BIRD occurred at the NASA Space Radiation Laboratory (NSRL) at Brookhaven National Laboratory in Upton, NY. We thank Chiara LaTessa, Adam Rusek, and Michael Sivertz for providing excellent support at NSRL. The NASA Advanced Exploration Systems Program provided support for the design, development, testing, integration, and data analysis of the BIRD. Additionally, the work was supported by NASA Bioastronautics Contract NAS9-02078. Contributions were also made by the University of Houston through Wyle Science Technology and Engineering Group Contract Number T72203.

The use of trademarks or names of manufacturers in this report is for accurate reporting and does not constitute an offical endorsement, either expressed or implied, of such products or manufacturers by the National Aeronautics and Space Administration.

Available from:

NASA Center for AeroSpace Information
7115 Standard Drive
Hanover, MD 21076-1320
443-757-5802

Abstract

This report summarizes the data acquired by the Battery-operated Independent Radiation Detector (BIRD) during Exploration Flight Test 1 (EFT-1). The BIRD, consisting of two redundant subsystems isolated electronically from the Orion Multi-Purpose Crew Vehicle (MPCV), was developed to fly on the Orion EFT-1 to acquire radiation data throughout the mission. The BIRD subsystems successfully triggered using on-board accelerometers in response to launch accelerations, acquired and archived data through landing, and completed the shut down routine when battery voltage decreased to a specified value. The data acquired are important for understanding the radiation environment within the Orion MPCV during transit through the trapped radiation belts.

Contents

1 Introduction **3**
- 1.1 Orion Multi-Purpose Crew Vehicle . . . 4
- 1.2 Exploration Flight Test 1 . . . 5

2 Detectors **6**
- 2.1 Battery-operated Independent Radiation Detector . . . 6
  - 2.1.1 Overview . . . 6
  - 2.1.2 Detector Description . . . 6
  - 2.1.3 Integration with Orion . . . 8
- 2.2 Radiation Area Monitor . . . 10
  - 2.2.1 Overview . . . 10
  - 2.2.2 Detector Description . . . 10
  - 2.2.3 Co-Location with Battery-operated Independent Radiation Detector . . . 10

3 Data Structures and Analysis **11**
- 3.1 Battery-operated Independent Radiation Detector . . . 11
- 3.2 Radiation Area Monitor . . . 12

4 Results **13**
- 4.1 Engineering Data . . . 13
  - 4.1.1 Acceleration Data . . . 13
  - 4.1.2 Battery Voltage . . . 15
  - 4.1.3 Temperature Data . . . 16
- 4.2 Radiation Data . . . 17
  - 4.2.1 Frame Occupancy and Rates . . . 17
  - 4.2.2 Dosimetry Rates . . . 18
  - 4.2.3 Model Comparisons . . . 21
  - 4.2.4 Dosimetry Rate Comparisons . . . 22
- 4.3 Accumulated Dose . . . 23
- 4.4 Altitude and Time Profiles . . . 24
- 4.5 Trajectory with Dosimetry . . . 26
- 4.6 Linear Energy Transfer Spectra . . . 29
- 4.7 Anisotropy . . . 30
  - 4.7.1 Directionality . . . 31
  - 4.7.2 Selection Criteria . . . 32
- 4.8 Frames of Interest . . . 35

5 Summary **39**
- 5.1 Detector Operation . . . 39
- 5.2 Data . . . 39
- 5.3 Model Comparisons . . . 39

6 References **41**

1 Introduction

The space environment poses many hazards to humans. Radiation is one of the most insidious of these hazards, as it is generally not detectable by human senses. Astronaut radiation exposure can be attributed to three major sources: galactic cosmic rays (GCR), solar particle events (SPE), and trapped particles. GCR consist of highly energetic nuclei of atoms from hydrogen to uranium and are present to some degree throughout the heliosphere regardless of orbit and mass or geomagnetic shielding. SPE consist primarily of protons of varying spectral characteristics (tens of MeV to a few GeV) and are usually highly attenuated by mass and geomagnetic shielding. Trapped particles consist of lower-energy electrons (maximum energy on the order of 10 MeV) and protons (maximum energy on the order of hundreds of MeV). They are a concern only in orbits around bodies with significant planetary magnetic fields, such as Earth. Radiation detectors are essential for characterizing these space radiation fields with the ultimate purpose of understanding the exposure to astronauts and the associated biological consequences [1, 2].

The Exploration Flight Test 1 (EFT-1) mission presented a unique opportunity to design, build, and test a space radiation detector utilizing the Timepix read-out chip technology [3–5]. Coupled with silicon semiconductors, the hybrid pixelated array detector allows the user to resolve charged particle energy deposition patterns, or clusters [6–12]. Detailed analysis of the clusters reveal information about the associated space radiation environment at an unprecedented level. While a unique opportunity, the EFT-1 flight presented challenges not typically encountered when integrating radiation detectors in vehicles intended for human use. Ultimately, the Advanced Exploration Systems (AES) RadWorks Radiation Environment Monitor (REM) team devised efficient means to overcome these challenges, successfully flying and recovering the Battery-operated Independent Radiation Detector (BIRD). This report presents an analysis of the data recovered from the BIRD. While a significant accomplishment, it represents only a fraction of the potential utility of the BIRD data.

1.1 Orion Multi-Purpose Crew Vehicle

The Orion Multi-Purpose Crew Vehicle (MPCV) is the primary vehicle that will support astronauts on exploration missions up to and including the Mars mission [13]. In contrast with the NASA's Space Transportation System (STS), or Space Shuttle, the capsule-based design harkens back to the days of Apollo. The Orion MPCV command module (CM) and service module (SM) are launched atop a rocket to reach Earth orbit. The Space Launch System (SLS) will be used for future exploration missions. Figure 1 shows how the various current NASA programs contribute to the Mars mission, including Orion and SLS.

NASA is pursuing a capability-driven approach to exploration, developing technologies required for the Mars mission and using them on preceding missions, regardless of destination [14]. Exploration radiation detection development embodies this approach, as Timepix-based detectors have been deployed on the International Space Station (ISS) since 2012 [15]. Developing and testing Timepix-based detectors for Orion MPCV missions is the next necessary step to establish operational history for this detection technology.

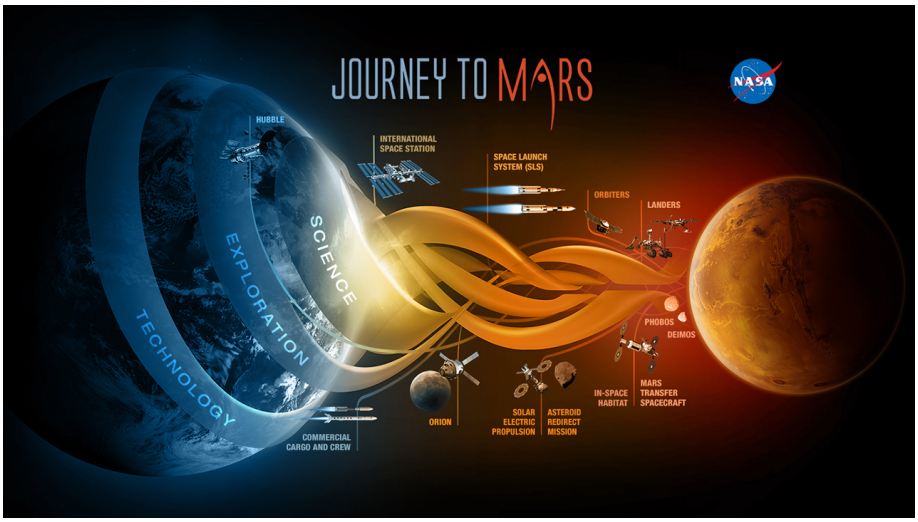

Figure 1: Journey to Mars [16].

1.2 Exploration Flight Test 1

The EFT-1 mission was the first opportunity to fly a Timepix-based detection system on the Orion MPCV. The Orion MPCV was launched from the Kennedy Space Center (KSC) atop a Delta IV Heavy rocket on December 5, 2014. The EFT-1 trajectory (shown in Figure 2) included two orbits: one low altitude orbit, and one highly eccentric orbit with an apogee of almost 6000 km. Although the primary mission objectives were to test the thermal protection system, hardware separation events, and the parachute system [17], the Orion MPCV passed through trapped electron regions and encountered intense regions of the trapped proton belts as a result of this flight profile. Radiation measurements in these regions are key to understanding astronaut radiation exposure in the Orion MPCV during trapped proton belt transit and comparing the trapped proton belt models with measurements.

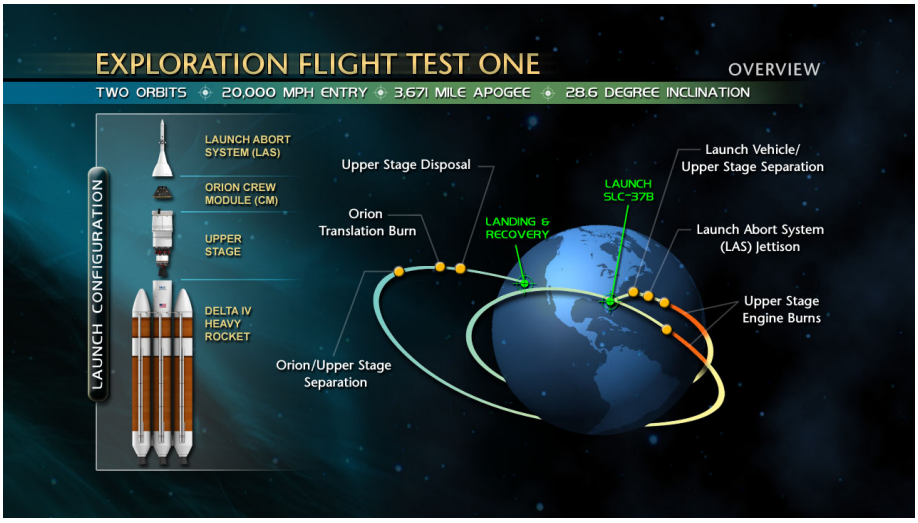

Figure 2: EFT-1 Overview [18].

2 Detectors

2.1 Battery-operated Independent Radiation Detector

2.1.1 Overview

Radiation monitoring is critically important for all future NASA crewed missions. One promising active detection method is the use of the modern semiconductor pixel detectors. These "radiation imaging" pixel detectors allow precise, time-resolved position and energy measurement in each pixel, resulting in a better understanding of the radiation environment during a mission. They can also be integrated into low-mass and low-power radiation monitoring systems, which are required for exploration class missions.

The BIRD is the first in-house developed radiation monitor based on this technology. It follows the successful REM Technology Demonstration, which is currently flying six Timepix-based radiation monitors on the ISS. It also serves as a precursor to the Hybrid Electronic Radiation Assessor (HERA), which is a distributed radiation monitoring system to be flown on future flights of the Orion MPCV.

2.1.2 Detector Description

The BIRD system is composed of two completely isolated and identical radiation instruments housed in the same mechanical enclosure (see Figure 3).

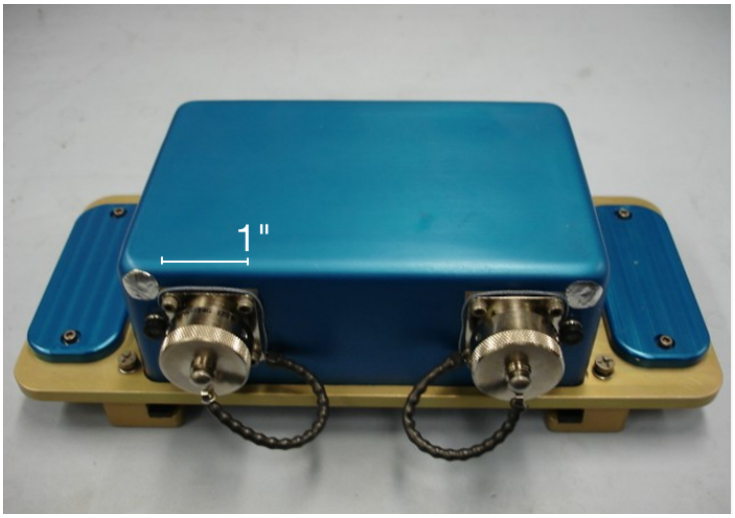

Figure 3: BIRD photo.

The two identical subsystems are separated by an aluminum partition and functioned similarly throughout the EFT-1 mission. Each instrument contains a battery assembly, a processor board, a power board, and a Timepix carrier board. The processor board consists of a digital signal processor, a Secure Digital (SD) memory card, an accelerometer, and other supporting electronics required to receive and store the radiation data from the Timepix assembly. The Timepix assembly is mounted permanently to the carrier board and connects to the processor board through a small connector. The serial peripheral bus provides primary communication between the signal processor and the Timepix assembly. The power board consists of a voltage boosting regulator and diode protection circuitry. The regulator receives the dynamic voltage input from the battery assembly and converts it into a steady and stable power source for all the other electronics. The carrier board is the interface to the Timepix. It has a small rear mount connector that plugs into the processor board. This board allows for easy installation and removal of the Timepix assemblies and serves as a test interface board, allowing for integration with a Fitpix (a Timepix data acquisition system developed by the Institute for Experimental and Applied Physics at Czech Technical University in Prague). Each instrument is equipped with a Military Specification (MIL spec) circular connector that can be used to interface with the outside world in order to perform system health and status checks before the flight. An exploded model of the device is shown in Figure 4.

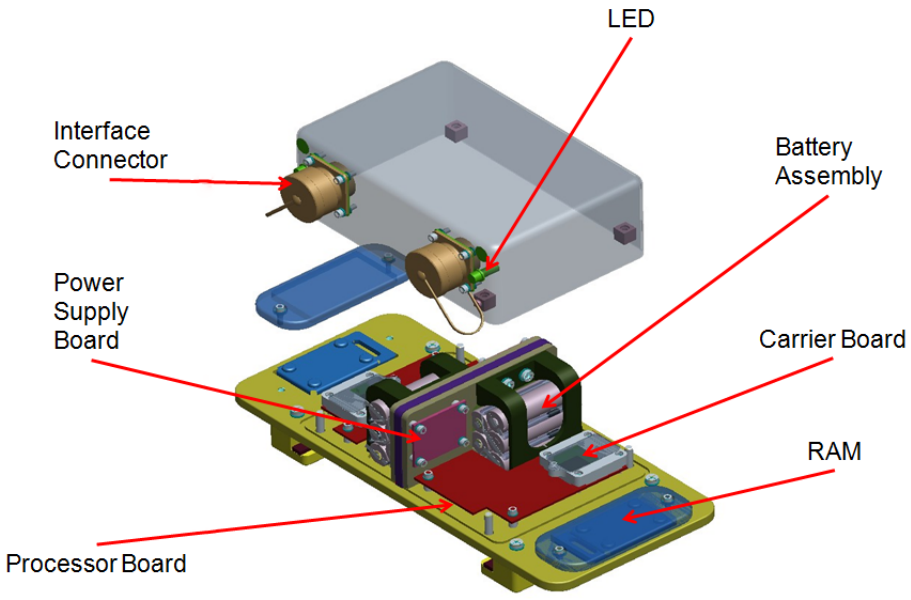

Figure 4: BIRD schematics.

During EFT-1, the BIRD operated as a stand-alone device. The measurements began after the BIRD accelerometer registered the required number of samples above a predefined acceleration value [19, 20]. The power was provided by internal batteries, and data were stored on the BIRD SD cards.

2.1.3 Integration with Orion

The AES RadWorks REM Team was engaged with the NASA Orion Program and Lockheed Martin throughout the design, testing, installation, flight, and deinstallation of BIRD. The BIRD was officially accepted, having met all levied requirements, by Lockheed Martin on October 21, 2013 [21]. Procedures and associated NASA Task Performance Sheets were delivered to Lockheed Martin to ensure a smooth integration process.

The BIRD Serial Number (S/N) 1001 and S/N 1002 units were delivered to KSC on October 7, 2014. The pre-flight functional check-out at KSC was performed on BIRD S/N 1001 on November 26, 2014, at which time the BIRD was placed in sleep mode. The Radiation Area Monitors (RAMs) were installed on the BIRD and then the BIRD was installed in the Orion MPCV on November 28, 2014, as shown in Figure 5. For reference, a Computer Aided Design (CAD) image of the installation is shown in Figure 6.

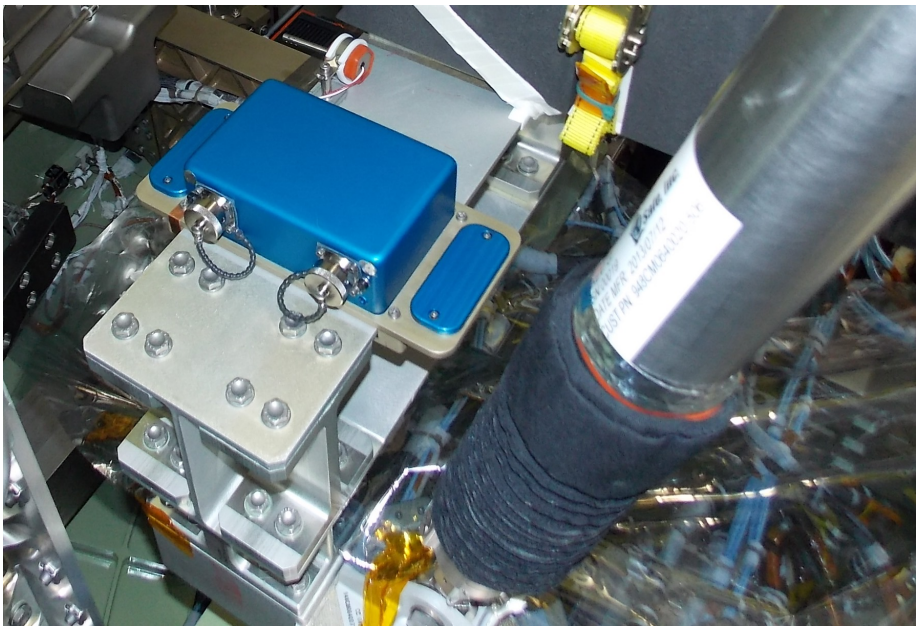

Figure 5: Image of BIRD installation.

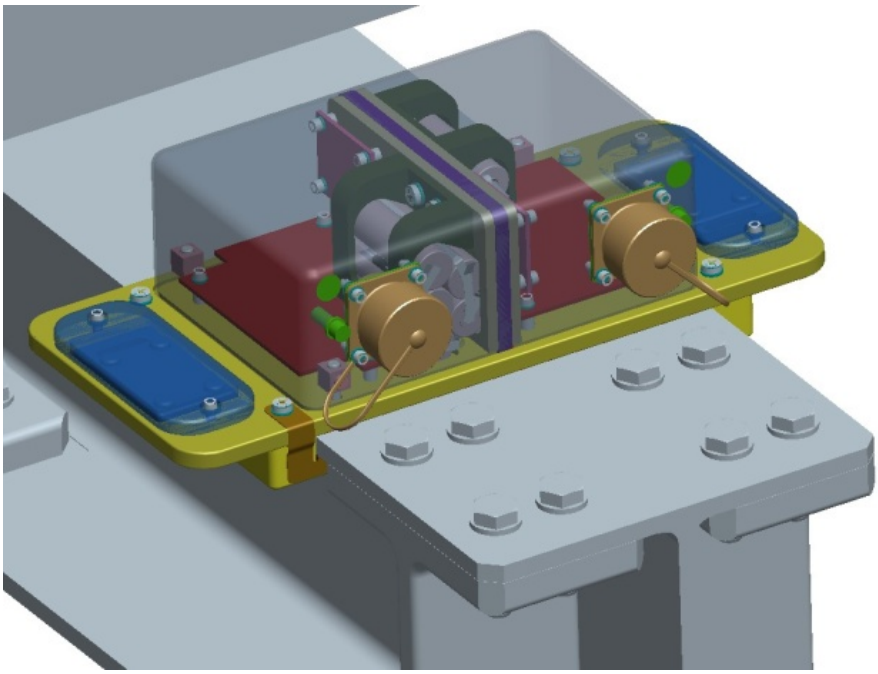

Figure 6: BIRD installation on MPCV.

2.2 Radiation Area Monitor

2.2.1 Overview

RAMs are passive radiation detectors that have been used extensively by NASA to monitor the radiation environment inside the ISS [22,23] and the Space Shuttle [24]. Measurements were also taken outside ISS as part of the Matroshka phantom through international collaboration with the German Aerospace Center [25]. During EFT-1, two RAM units were attached to the BIRD instrument to provide for direct comparison of the radiation absorbed dose data of the BIRD to the RAM passive detectors. In addition, three RAM Control units were provided to account for the background radiation during shipping and transportation to and from the EFT-1 launch and landing sites.

2.2.2 Detector Description

RAMs consist of a suite of thermoluminescence (TL) and optically stimulated luminescence (OSL) dosimeters co-located inside the RAM to provide an accurate description of the radiation environment in terms of total mission dose. The general operating principle for the TL/OSL processes involves emission of light (i.e., photon counts) after an external stimulation (i.e., by heat or light) of a previously irradiated dosimeter [26, 27]. The integral of the luminescence signal coming from the TL/OSL dosimeters over the stimulated period is proportional to incident radiation absorbed dose, thus allowing the TL/OSL detectors to be successfully used for radiation dosimetry measurements. The following TL and OSL materials were included in the the RAM Flight and Control units: LiF: Mg,Ti (TLD-100); ^{6}LiF: Mg,Ti (TLD-600); ^{7}LiF: Mg,Ti (TLD-700); CaF_2:Tm (TLD-300); and Al_2O_3:C (Luxel).

2.2.3 Co-Location with Battery-operated Independent Radiation Detector

As shown in Figure 4, the BIRD baseplate was designed to house two RAMs. Each RAM was secured with an aluminum cover with a thickness approximately equal to that of the BIRD housing. The purpose of the RAMs was to allow for comparison of the BIRD dosimetry results with a device that has ISS and STS heritage. Although the BIRD detectors and RAMs are located near one another, future analyses will include shield distribution analysis to account for local variation in the radiation field due to differential shielding.

3 Data Structures and Analysis

3.1 Battery-operated Independent Radiation Detector

The Timepix detectors used in the BIRD take periodic samples of the radiation environment. To start the sample, the Timepix is commanded to start acquisition. This is analogous to opening the shutter of a camera. Charged particles interacting in the sensitive volume of the detector deposit energy in the sensor, which causes counts to be registered in the associated pixels. Once the frame acquisition is terminated, the array of pixel counts is read out and stored as a matrix. Charged particle interactions result in clusters of pixels, which are two-dimensional projections of the charged particle track through the detector convolved with a detector response function.

Reference [15] provides a comprehensive summary of Timepix-based data structures and analysis; an adapted excerpt of the relevant information for BIRD data structures and analysis to obtain absorbed dose and dose equivalent information is provided below.

Raw data are processed and converted to a ROOT-based [28] data format containing the original pixel Time-Over-Threshold data and the calibrated energy-per-pixel map data with the associated meta-data for each frame. Orbital location, absorbed dose, absorbed dose rate, dose equivalent, dose equivalent rate, and non-zero pixel count are also calculated for each frame.

One of the primary requirements for the data conversion is correlation of the timestamp from a given data frame to an orbital location. The orbital location and timestamp association for EFT-1 was achieved using a combination of planned trajectory provided by Lockheed Martin to AES RadWorks and the as-flown trajectory from CM/SM separation to landing. This allows the timestamp from each data frame to be associated with a latitude, longitude, and altitude for each frame.

In addition to applying the energy calibration information to convert Time-Over-Threshold measurements to energy deposition data for each individual pixel in each of the BIRD subsystems [29], the processing routine also performs basic cluster identification operations and then calculates polar angle, azimuthal angle, total energy deposited, and dE/dx for each incident particle track [11]. Absorbed dose, absorbed dose rate, dose equivalent, and dose equivalent rate are also calculated for each frame on a track-by-track basis and stored within the ROOT data tree.

References [11] and [15] detail the Ground Analysis Software Calculations, but a brief review is warranted for the quantities discussed in this work. Dose in silicon (Equation 1) for each track, $D_{t,Si}$, is determined from the sum of calibrated energy values E_p for each pixel i in the track and the mass of the silicon sensor bonded to the Timepix chip. The dose per frame is the sum of the track doses within a given frame.

$$D_{t,\mathrm{Si}} = \frac{1}{m_{sensor}} \cdot \sum_{p_i} E_{p_i} \tag{1}$$

Conversion from dose in silicon to dose in water is accomplished for each track using an energy dependent factor with an asymptotic limit of 1.23 (Equation 2). The conversion factor is calculated based on the ratio of stopping powers for water and silicon, with stopping powers estimated based on track dE/dx.

$$D_{t,\mathrm{H_2O}} = D_{t,\mathrm{Si}} \cdot C\left(dE/dx_t\right) \tag{2}$$

Since each frame has an associated collection period, dose rate is easily calculated for an individual frame from the dose in the frame divided by the recorded collection time for that frame. Dose rate per minute is calculated by dividing the sum of the dose per frame, F, by the sum of the acquisition time, t_{acq}, for the data acquired in minute interval i (Equation 3).

$$\dot{D}_{i,\mathrm{H_2O}} = \frac{\sum_{F,i} D_{F,\mathrm{H_2O}}}{\sum_{F,i} t_{acq}} \tag{3}$$

Dose equivalent estimates are found on a track-by-track basis under the assumption that dE/dx in water for each track is equivalent to the unrestricted Linear Energy Transfer (LET) in water. The LET value is then used in conjunction with the ICRP 60 [30] parameterization for quality factor to calculate the dose equivalent value for the track.

3.2 Radiation Area Monitor

The two RAM Flight units and the three RAM Control units have been processed post-flight in the Space Radiation Dosimetry Laboratory at the Johnson Space Center. The TL and OSL measurements were performed using two automated Harshaw 5500 TL and Risø TL/OSL DA-15C/D readers and followed particular heating temperature and light stimulation profiles as described in Reference [23]. The TL/OSL dosimeters have been calibrated using a ^{137}Cs gamma source and the reported quantity is the gamma dose to water, $D^{RAM}_{\mathrm{H_2O}}$, calculated as shown in Equation 4

$$D^{RAM}_{\mathrm{H_2O}} = D_{^{137}\mathrm{Cs}} \cdot \frac{S_{RAM}}{S_{^{137}\mathrm{Cs}}} \tag{4}$$

where S_{RAM} is the luminescence signal after EFT-1 and $S_{^{137}\mathrm{Cs}}$ is the luminescence signal after a ^{137}Cs exposure of absorbed dose $D_{^{137}\mathrm{Cs}}$. The final dose for each RAM attached to BIRD was calculated by finding the difference between $D^{RAM}_{\mathrm{H_2O}}$ and the Control RAM absorbed dose, $D^{RAM}_{Control}$, as shown in Equation 5.

$$D^{RAM}_{EFT-1} = D^{RAM}_{\mathrm{H_2O}} - D^{RAM}_{Control} \tag{5}$$

4 Results

The first part of this section is dedicated to engineering data measured by the BIRD during the EFT-1 flight. The exhibited quantities were chosen because they had the potential to impact the operation of the instrument and quality of the radiation data. The engineering data are shown from the start of BIRD data acquistion to BIRD shutdown[1]. Readers will note that "Left" and "Right" are used to differentiate the data from the two BIRD subsystems. This designation refers to the subsystem on the side of the BIRD when viewed facing the connectors on the BIRD housing, as shown in Figure 3.

In the remainder of this section, the results of the data analysis (Section 3) as applied to the BIRD data during EFT-1 are presented. More specifically, only the radiation data relevant to the flight from the start of BIRD data acquistion to Orion MPCV splashdown are presented[2]. Unless otherwise noted, all dosimetry quantities are represented in water.

4.1 Engineering Data

Acceleration measurements, battery voltage, and temperature measurements are shown from below, from the start of BIRD data acquisition to BIRD shutdown.

4.1.1 Acceleration Data

Acceleration data from the two BIRD tri-axis accelerometers are shown in Figure 7. The magnitude of the acceleration vector is the plotted quantity. The first peak, just shy of 4g, corresponds to accelerometer measurements just after the start of BIRD data acqusition, which occurred about 2 minutes after lift-off. The smaller peak just after the first peak corresponds to the Second Stage #1 ignition. At about 14:00 Coordinated Universal Time (UTC), another small peak is observed, corresponding to Second Stage #2 ignition. The highest acceleration data (around 8g) are observed at parachute deploy. After splashdown, the BIRD accelerometers measured a value of approximately 1g, as expected, since BIRD was subjected to Earth's gravity. Accelerometer data will be used to perform an absolute calibration of the BIRD real-time clock when the entire as-flown trajectory for EFT-1 becomes available.

[1] December 5, 2014 at 12:07:05 UTC to 22:11:29 UTC.
[2] December 5, 2014 12:07 UTC to 16:30 UTC

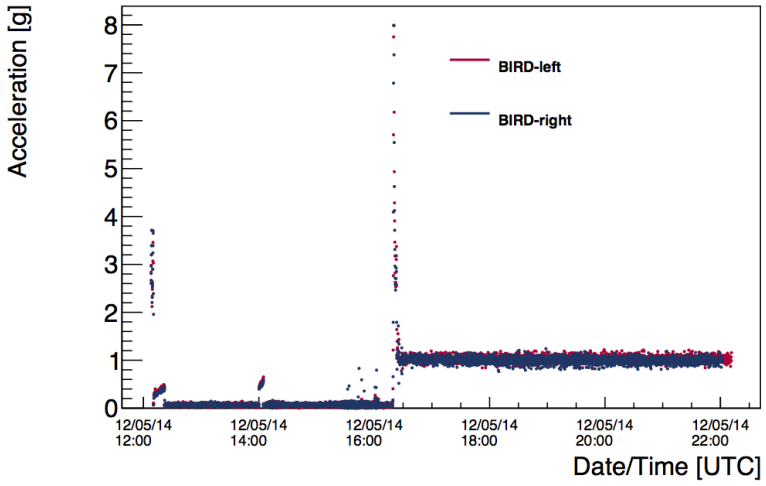

Figure 7: Acceleration as measured by BIRD.

4.1.2 Battery Voltage

Voltage measurements for the BIRD battery packs from the two BIRD voltmeters are shown in Figure 8. The measurements began at the start of BIRD data acquisition and ended when the BIRD subsystems performed the shutdown routine. The shutdown routine was triggered when the BIRD battery pack voltage decreased to 2 V. The qualitative shape of the battery pack voltage as a function of time is very similar to that expected for Energizer L91 batteries [31].

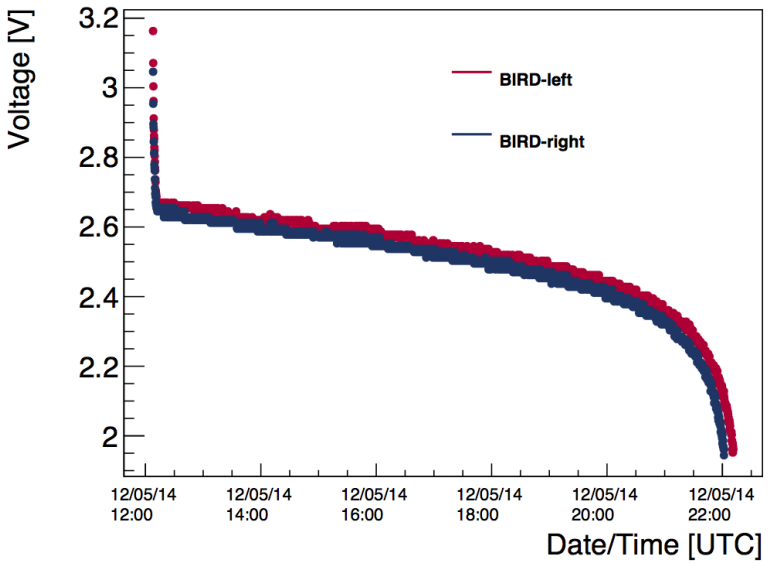

Figure 8: BIRD battery pack voltage during flight.

4.1.3 Temperature Data

BIRD subsystem temperature data are shown for the accelerometer (Figure 9) and the memory (Figure 10). Throughout the flight, the temperature for the Right subsystem exceeded the temperature for the Left subsystem. The offset appears to be about 2°C for both sets of temperature sensors. BIRD temperature data will be coupled with EFT-1 ambient temperature measurements (as available) to refine thermal math models for future detector development.

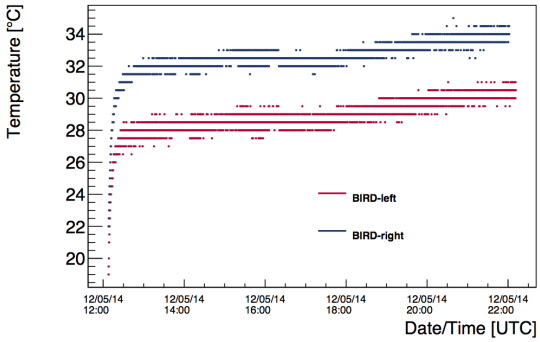

Figure 9: Temperature as measured on BIRD accelerometer.

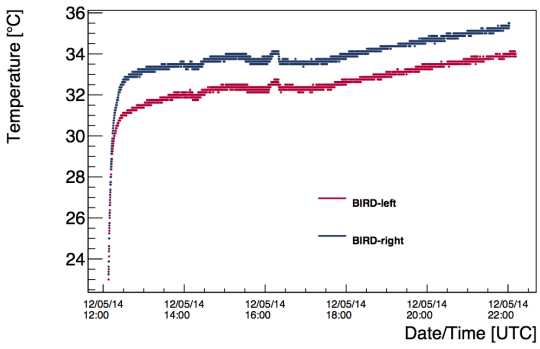

Figure 10: Temperature as measured on BIRD memory.

4.2 Radiation Data

4.2.1 Frame Occupancy and Rates

Figure 11 provides the frame occupancy and recorded frame rate per minute. Note that around 15:20 UTC, the frame rate rapidly increases and saturates at around 180 frames/minute while the frame occupancy sextuples[3]. This demonstrates the instrument's ability to accurately sample complex environments with many particles. Here, occupancy is defined as the number of pixels with energy deposition normalized by the number of pixels in the sensor. The largest occupancy spike (c.f. Figure 11) occurs between 15:40 UTC and 16:00 UTC and contains a high number of overlapping particle tracks.

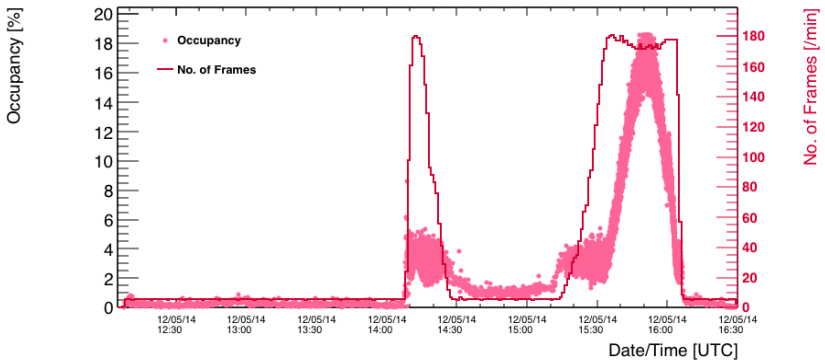

(a) Occupancy and frame rate for the left detector.

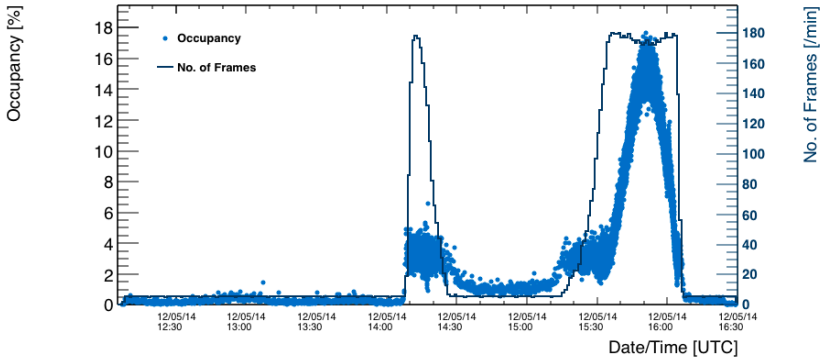

(b) Occupancy and frame rate for the right detector.

Figure 11: Frame occupancy and the number of recorded frames per minute for BIRD during EFT-1.

[3]The observed saturation is driven by the speed of the SD-card used to store data.

4.2.2 Dosimetry Rates

Absorbed dose rates and dose equivalent rates for EFT-1 are provided in Figure 12 and Figure 13, respectively. There are two large peaks in the absorbed dose rate plot; they occur between approximately 14:10 UTC to 14:20 UTC and 15:20 UTC to 16:05 UTC. The occupancy during the first peak rarely exceeded 5%, but occupancy increased to greater than 18% during the second peak. To reiterate, occupancy is the number of pixels with recorded energy deposition normalized by the total number of pixels in a frame, and at large occupancies, there are many overlapping particle tracks. These overlaps do not affect the calculation of absorbed dose, but they do affect the calculation of dose equivalent.

Currently, our algorithms and analyses are still at an early stage of development and cannot correctly distinguish all of the individual particle tracks in these overlap regions. Unfortunately, the minimum frame length limit was set too high; this has been corrected for future missions, as the Timepix is capable of operating with frame durations substantially shorter than 100 ms. The techniques and algorithms perform better with substantially shorter frame times, where overlapping tracks are less frequent. The quality factor [30] used to calculate dose equivalent is dependent on LET, and hence is dependent on energy and particle type. Misidentifying the number of particle tracks in a high occupancy frame as a single track leads to an overestimate of the quality factor for this environment. Presently, we have assumed that the fields in the first and second peaks are qualitatively similar and so we have characterized the quality factor from the second peak using the quality factor from the first peak. This method was used for the data shown in Figure 13 and all other figures showing dose equivalent. An update to the particle separation algorithms is expected later this year.

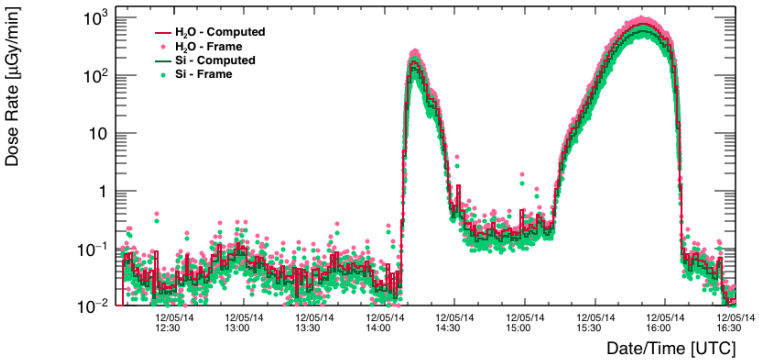

(a) Dose rate in water for the left detector.

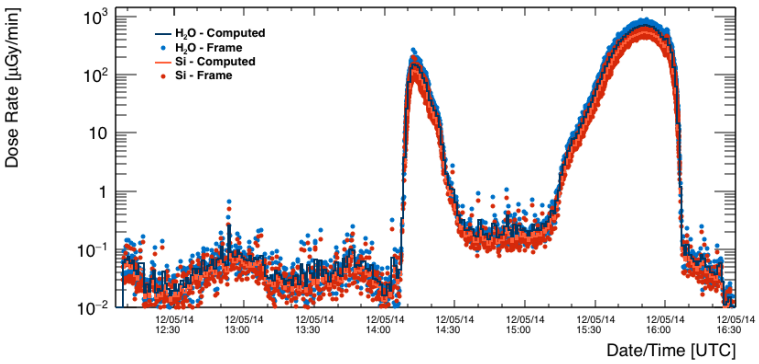

(b) Dose rate in water for the right detector.

Figure 12: Dose rate in silicon and water (H_2O) for each frame (dots) and computed using equation 3, where the sum is over a 1-minute period (solid line).

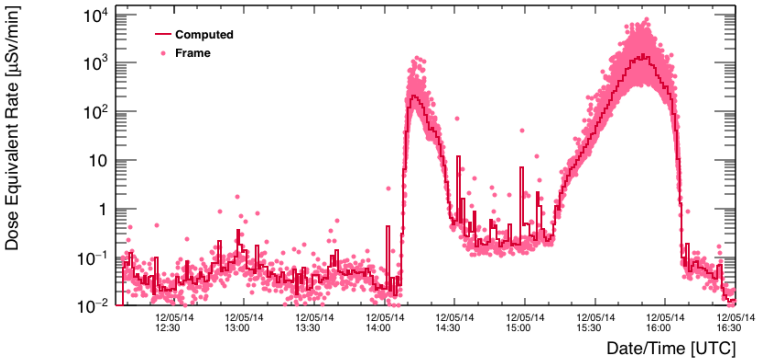

(a) Dose equivalent rate in water for the left detector.

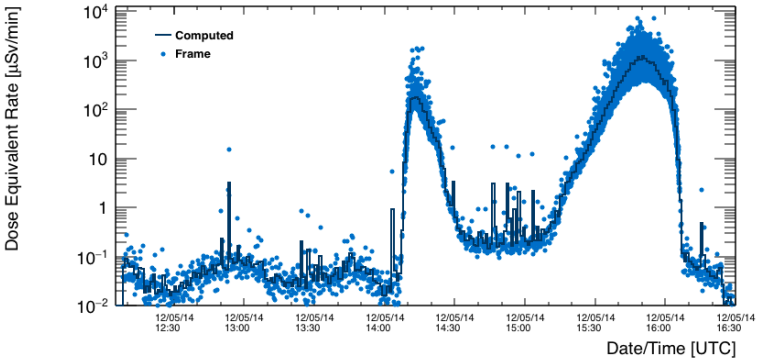

(b) Dose equivalent rate in water for the right detector.

Figure 13: Dose equivalent rate for each frame (dots) and computed using equation 3, where the sum is over a 1-minute period (solid line).

4.2.3 Model Comparisons

The AP (energetic proton) and AE (energetic electron) models have been developed to specify the radiation environment for modern spacecraft design applications. The latest generations of these models - AP9 and AE9 - offer unprecedented coverage in particles and energies that address the major space environmental hazards and include uncertainties and dynamics that have never been available for use in design [32]. Figure 14 shows data-model comparisons between BIRD and AP9/AE9. Initial comparisons between BIRD data and AP9/AE9 (AX9) show very good agreement for an estimated shielding thickness of 10 g/cm^2 of aluminum. Future work will use the as-flown trajectory to account for Orion's rotation along its flight path. CAD shielding analysis will be performed to fully characterize the vehicular shielding distribution surrounding the detector locations. These modifications will lead to more informative data analyses and model comparisons.

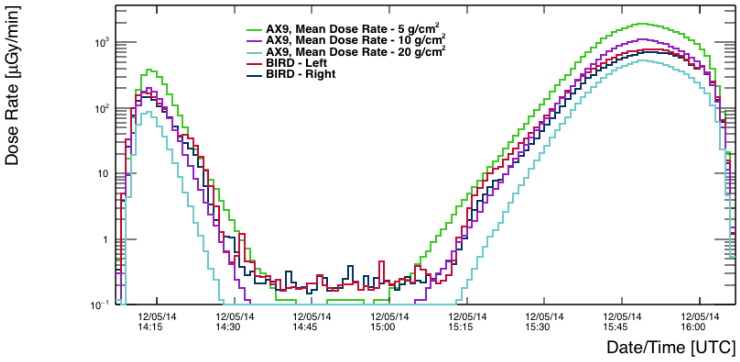

Figure 14: BIRD dose rates and AX9 mean dose rates at varying thicknesses.

4.2.4 Dosimetry Rate Comparisons

Dosimetry rate comparisons between the left and right detectors of BIRD are shown in Figure 15. The agreement between the absorbed and equivalent doses is nearly linear; some deviation is expected since each detector sees a slightly different radiation environment. For example, one side may observe heavy ions or interactions, while the other may not. This is also evident in Table 1, which presents the total dose accumulated by the BIRD and RAM instruments during EFT-1.

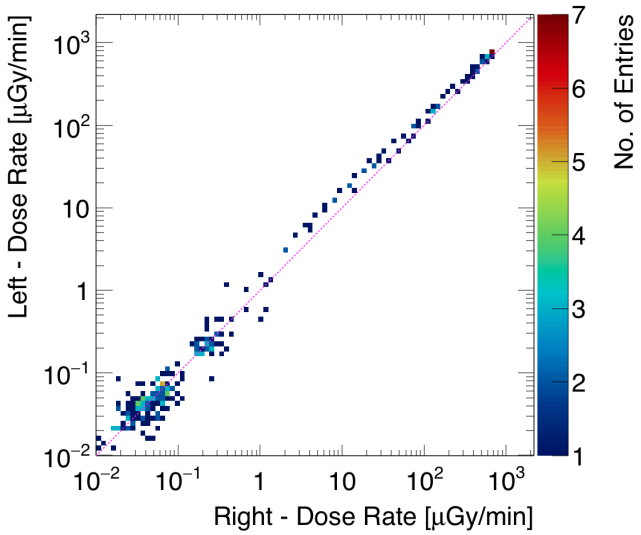

(a) Absorbed dose rate comparison.

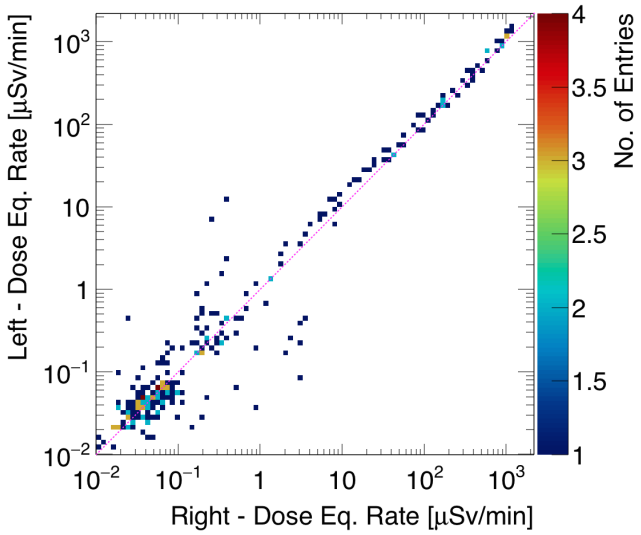

(b) Dose equivalent rate comparison.

Figure 15: Absorbed dose rate and dose equivalent rate comparisons between the Left and Right BIRD subunits. The magenta dashed line represents y=x.

4.3 Accumulated Dose

Cumulative absorbed dose during EFT-1 is provided in Figure 16; the totals for the mission are located in Table 1.

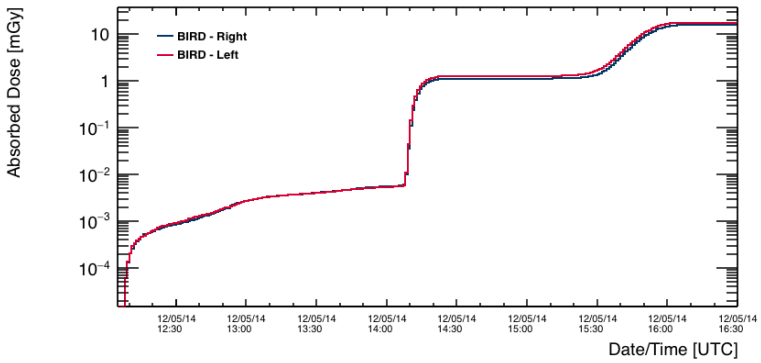

Figure 16: Cumulative absorbed dose (in water) for BIRD during EFT-1.

The total absorbed dose for EFT-1 as measured by BIRD subunits and the associated RAMs are located in Table 1. The RAM absorbed doses represent the average for the individual TL/OSL dosimeters corresponding to each of the two RAM flight units, together with the standard error of the mean. The Left RAM and Right RAM TL/OSL dosimeter individual absorbed dose values had standard deviations of 5% and 4%, respectively.

Table 1: Total absorbed dose for BIRD and RAMs aboard Orion MPCV and ISS-Tissue Equivalent Proportional Counter (TEPC) during EFT-1 on December 5, 2014 between 12:07 UTC and 16:30 UTC.

	BIRD [mGy]	RAM [mGy]		ISS-TEPC [mGy]
Left	17.9	15.1 ± 0.3		0.015
Right	15.7	13.5 ± 0.2		

4.4 Altitude and Time Profiles

In this subsection, dosimetric quantities are presented as a function of altitude and time. The highest observed dose rates did not occur at the peak altitude, but instead occurred before and just after the peak altitude. This observation is explained by the changes in the spectral characteristics of the trapped radiation field along the trajectory; while still within the trapped belt region, the spectrum was comprised of lower-energy protons in the lower dose region between the two dose rate peaks.

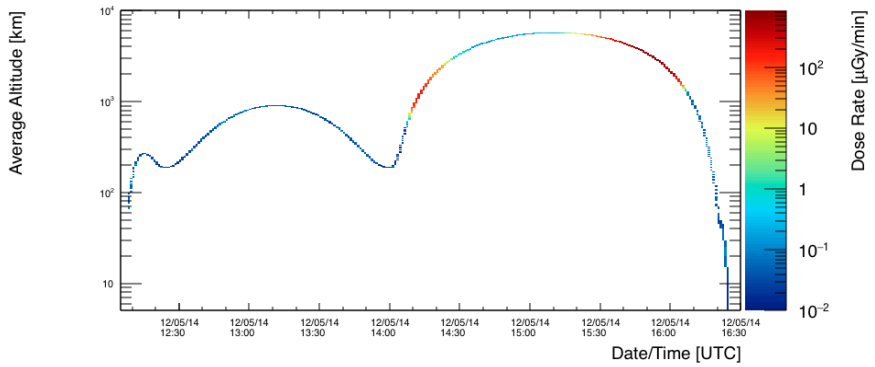

(a) Absorbed dose rate as a function of altitude and time for the left detector of BIRD.

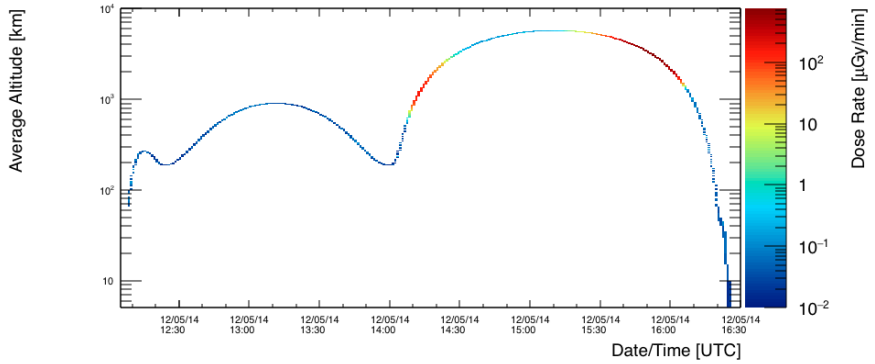

(b) Absorbed dose rate as a function of altitude and time for the right detector of BIRD.

Figure 17: Altitude as a function of time, weighted by the measured dose rate in EFT-1 trajectory.

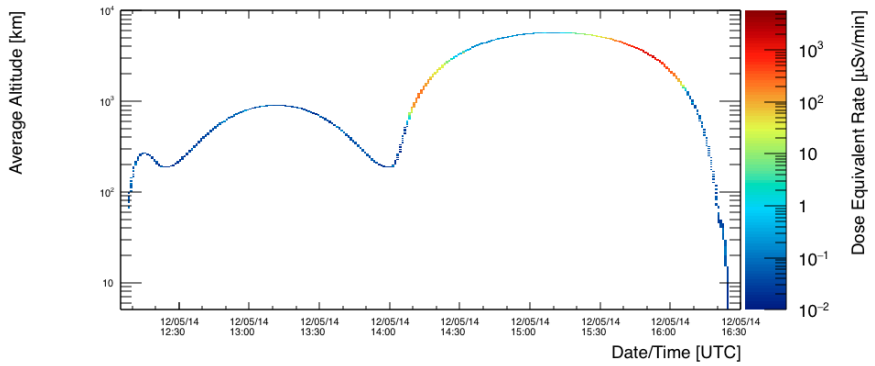

(a) Dose equivalent rate as a function altitude and time for the left detector of BIRD.

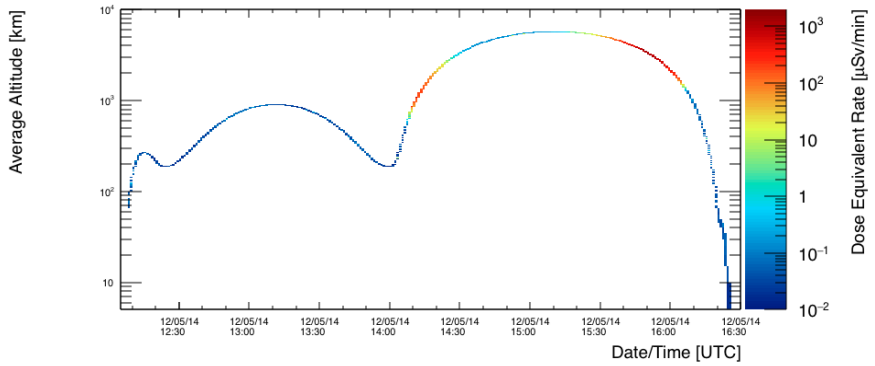

(b) Dose equivalent dose rate as a function of altitude and time for the right detector of BIRD.

Figure 18: Altitude as a function of time, weighted by the dose equivalent rate in EFT-1 trajectory.

4.5 Trajectory with Dosimetry

Dosimetric quantities as a function of the Orion MPCV trajectory are presented in this subsection. A high-definition video of the Orion MPCV trajectory with absorbed dose rate is available to readers using Adobe Reader, as shown in Figure 21.

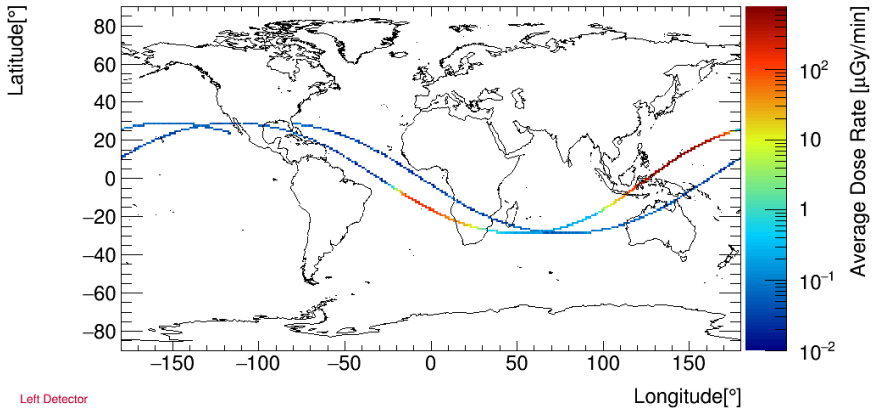

(a) Absorbed dose rate as a function of EFT-1 trajectory for the left detector of BIRD.

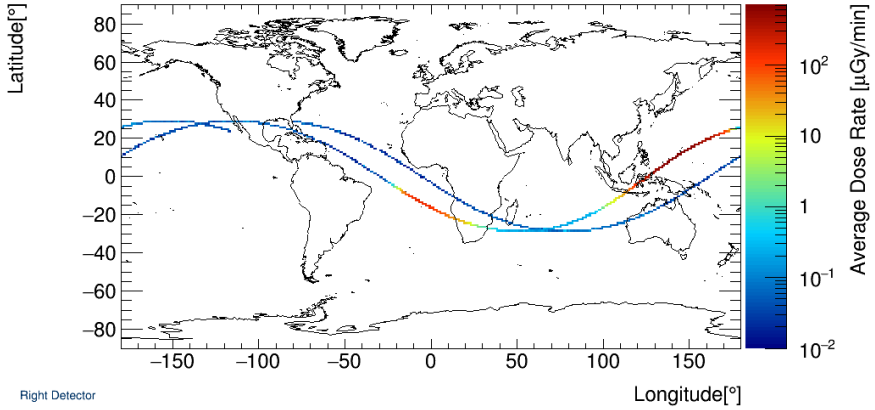

(b) Absorbed dose rate as a function of EFT-1 trajectory for the right detector of BIRD.

Figure 19: Dose rate as function of EFT-1 trajectory.

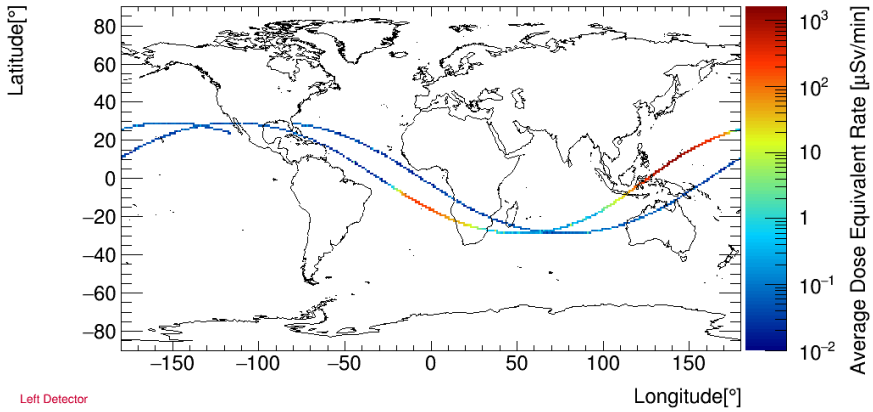

(a) Dose equivalent rate as a function of EFT-1 trajectory for the left detector of BIRD.

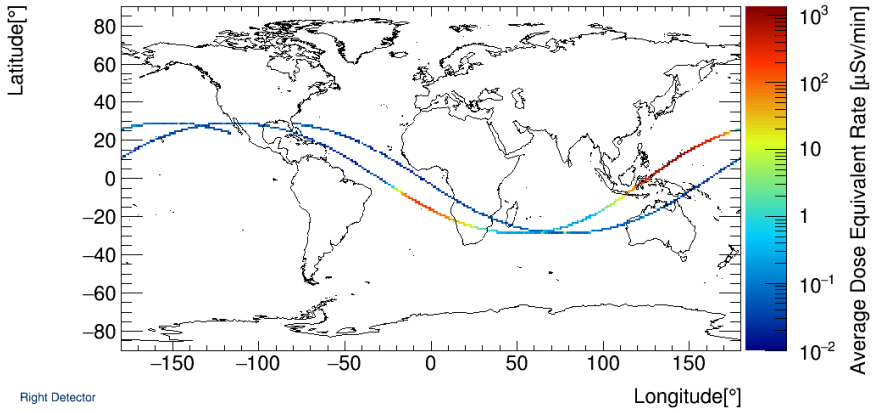

(b) Dose equivalent dose rate as a function of EFT-1 trajectory for the right detector of BIRD.

Figure 20: Dose equivalent rate as function of EFT-1 trajectory.

After analysis, the BIRD data were reformatted for use in Google Earth Pro [33]. Figure 21 illustrates the absorbed dose rate along EFT-1's highly eccentric orbit. Readers can open this document in Adobe Reader and click on the image to play/pause the video. Note that the center of the video reflects the position of Orion MPCV along the trajectory path.

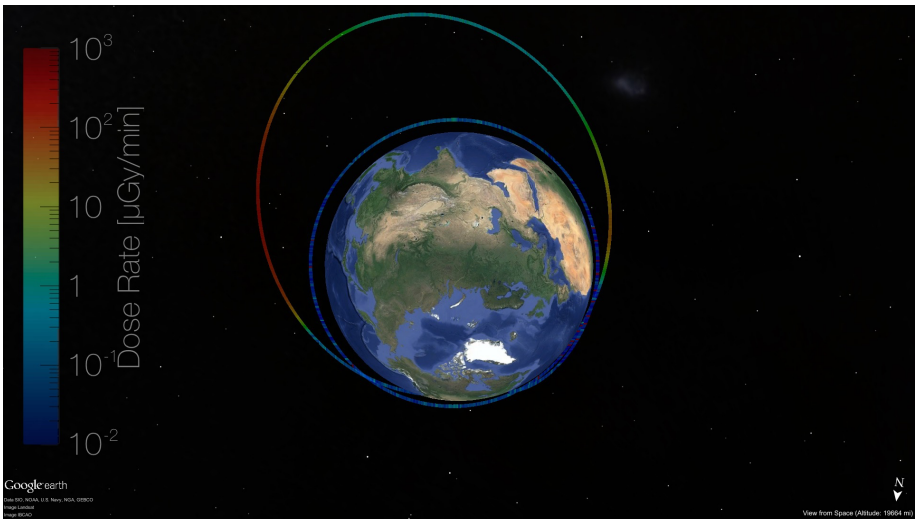

Figure 21: Dose rate in water [μGy/min] for the right detector of BIRD as a function of EFT-1 trajectory.

4.6 Linear Energy Transfer Spectra

LET spectra (in silicon) were generated for each BIRD subunit based on calculation of individual ion energy deposition and track length through the detector. The results below exclude portions of the trajectory where the pixel occupancy exceeds 8% in order to reduce track overlaps.

The results, shown in Figure 22 for both BIRD units for the full mission duration but excluding the high occupancy frames, display characteristics and overall shapes consistent with one another. The results are also similar to spectra generated by REM units aboard ISS. This includes a small peak at approximately 14 keV/μm, which corresponds to protons with energies low enough to stop within the detector volume.

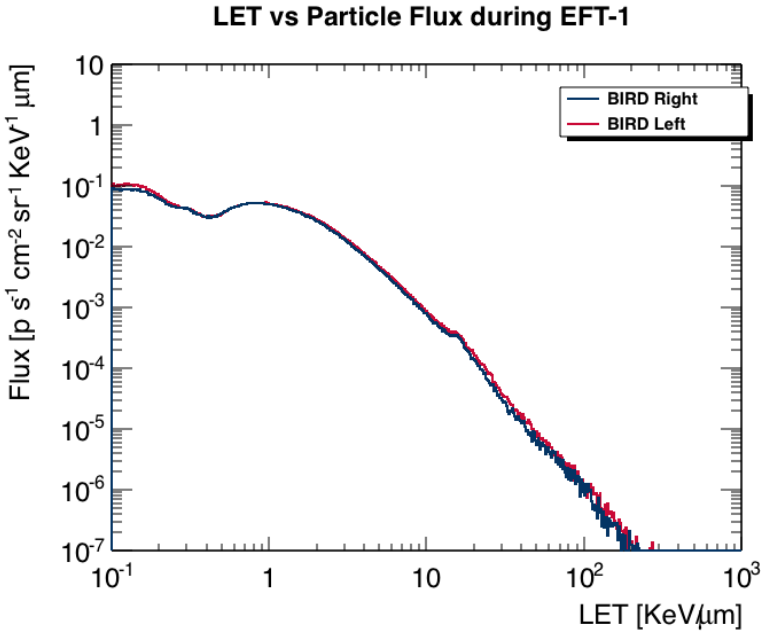

Figure 22: Number of particles as a function of LET.

4.7 Anisotropy

An excerpt from "Space radiation dosimetry in low-Earth orbit and beyond" [34] succinctly summarizes particle anisotropy:

> The proton flux encountered by a spacecraft as it traverses the SAA is anisotropic. Protons traveling toward the east are following geomagnetic field lines (or guiding centers) above the spacecraft's orbit, while protons traveling toward the west are following geomagnetic field lines that lie below the spacecraft's orbit. The radius of the cyclotron motion of energetic protons in the SAA is of the same order as the height of the atmosphere (atmospheric density scale height). Particles traveling toward the west traverse a significantly denser portion of the atmosphere than do particles traveling toward the east and are thereby more likely to undergo interactions with the atmosphere and be attenuated. This phenomenon is referred to as the east/west trapped proton anisotropy. For spacecraft such as the Space Shuttle that typically have no fixed orientation relative to the geomagnetic field when they pass through the SAA, the effects of the trapped proton anisotropy tend to be averaged out over the duration of the mission. For spacecraft such as ISS that are in a fixed orientation relative to the geomagnetic field, the east/west trapped proton anisotropy can lead to differences of up to a factor of 3 in dose rate between the west and east sides of the spacecraft.

During EFT-1, the Orion MPCV flew through one low-altitude orbit and one highly eccentric orbit with an apogee of almost 6000 km. During this mission, the Orion MPCV did not pass through the trapped belts at altitudes similar to the ISS (the South Atlantic Anomaly, or SAA). The BIRD is unique to other space radiation instrumentation currently in use by NASA for crew health and safety, as it provides particle directionality by means of pixel detector technology. With proper data analysis, directional information from the environment can be reconstructed. Particle directionality is especially observed in the trapped radiation belts.

Theory predicts that for low altitudes, particle flux at lower altitudes in the trapped proton region should be anisotropic due to atmospheric shielding. For altitudes above about 1800 km, the environment should be more isotropic. The present analysis is complicated by the fact that the vehicle was rotating during certain portions of the flight. Despite this complication, the data appear to indicate directionality at lower altitudes and a more isotropic environment at higher altitudes within the trapped proton region.

4.7.1 Directionality

The BIRD coordinate system is illustrated in Figure 23. The azimuthal angle - ϕ and polar angle - θ respectively correspond to the angle between the X and Y axes (e.g., in the sensor plane) and Z and X axes (normal to the sensor plane).

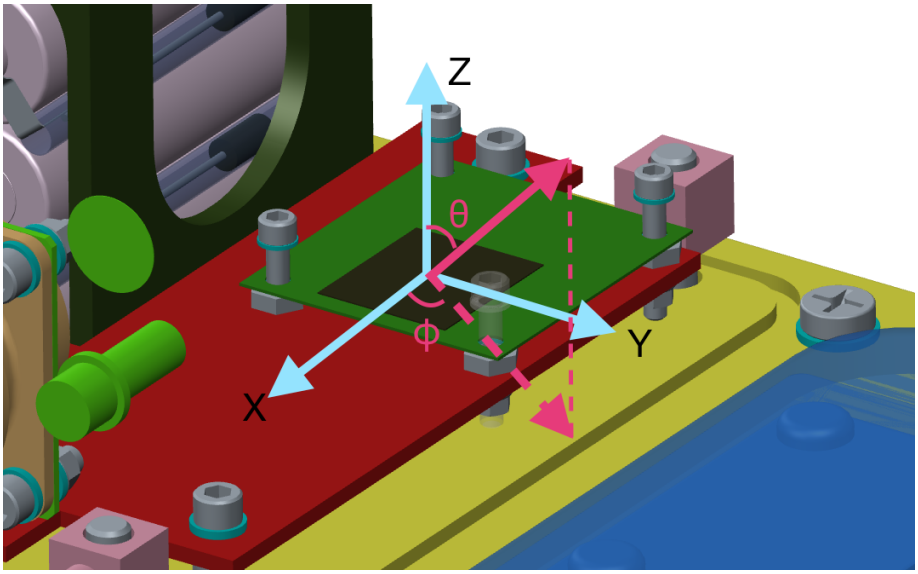

Figure 23: BIRD coordinate system.

A preliminary look at the data shows that there is clear directionality, as shown in Figure 24.

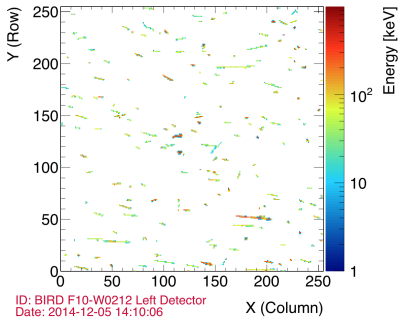

(a) Particle track directionality in the left detector during the first peak in dose rates.

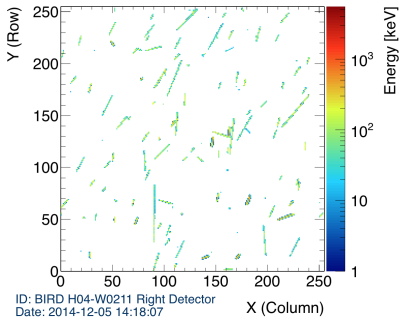

(b) Particle track directionality in the right detector during the first peak in the dose rates.

Figure 24: Example particle track directionality in the BIRD detector.

4.7.2 Selection Criteria

For our preliminary analysis of directionality, we applied a simple set of selection criteria to reduce the number of overlapping tracks at high altitudes and to address other algorithm shortcomings. These criteria are explained below.

- $0.015 < |\phi| < 1.555$ - Select tracks that are not parallel to columns or rows of pixels.
- $\theta > 0.008$ - Select tracks that are not normal to the sensor plane.
- Cluster Size > 4 pixels - Select tracks large enough to properly reconstruct angular information.
- Frame Occupancy < 0.08 - Select frames for which no more than 8% of the pixels are above threshold.

Figure 25 shows the azimuthal angular distribution as a function of time in the left detector with the selection criteria applied. Directionality is observed in Figure 25b, a lower-altitude region of the trajectory, while the distribution shown in Figure 25c, a higher-altitude region of the trajectory, appears largely isotropic. These observations roughly correspond to what is expected for the trapped proton environment from theory.

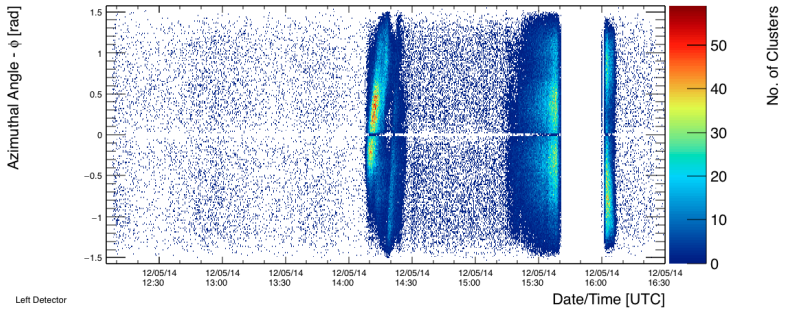

(a) Azimuthal angle - ϕ distributions as a function of time in the left detector.

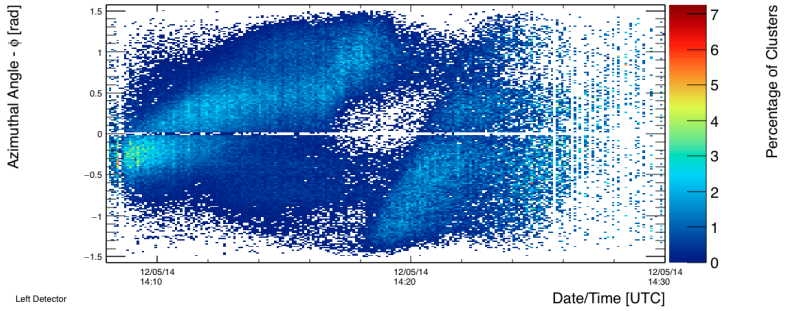

(b) Azimuthal angle - ϕ distributions during the first peak in dose for the left detector.

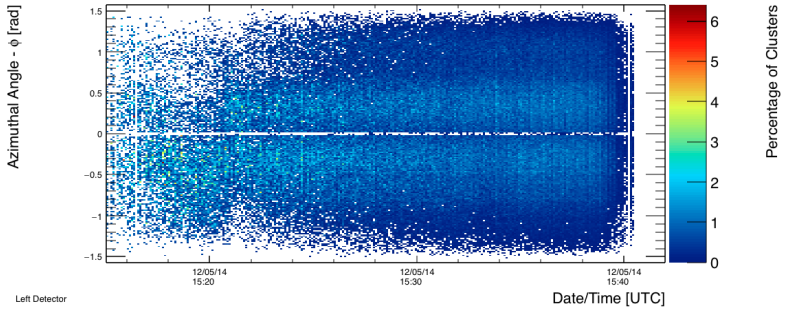

(c) Azimuthal angle - ϕ distributions before the second peak in dose for the left detector.

Figure 25: Azimuthal angle - ϕ distributions during different periods of EFT-1 for the left detector.

As we examine specific time periods in the data, we can see that the directionality changes as a function of our trajectory, as shown in Figure 26.

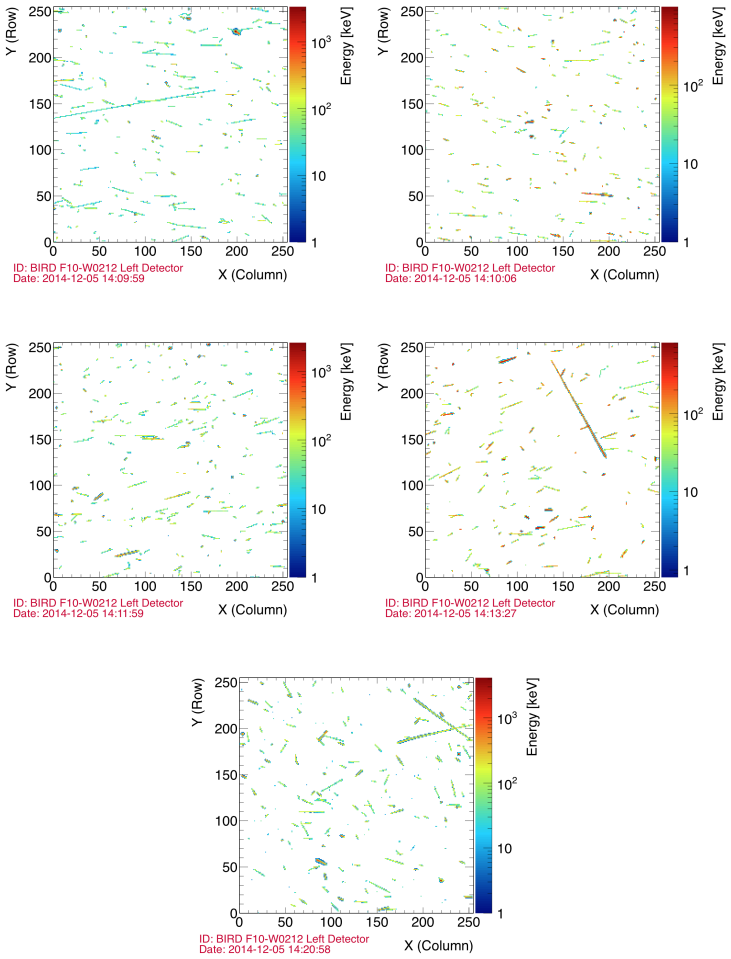

Figure 26: Directionality of tracks in the left detector during the first peak in dose rates (Figure 25b).

4.8 Frames of Interest

The frames of interest shown in this subsection are observed to have two primary types of particle phenomena: interactions and heavy ions. These phenomena result in higher dose equivalent rates. Tags have been placed on the dose equivalent rate for EFT-1 in Figure 27. These tags correspond to the frames shown in Figures 28 - 32.

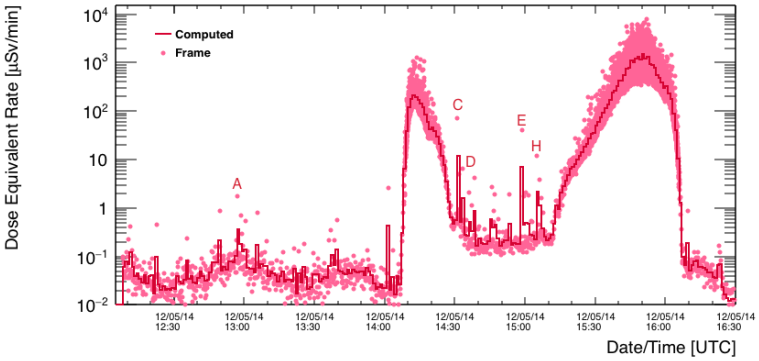

(a) Dose equivalent rate for the left detector, tagged for frames shown below.

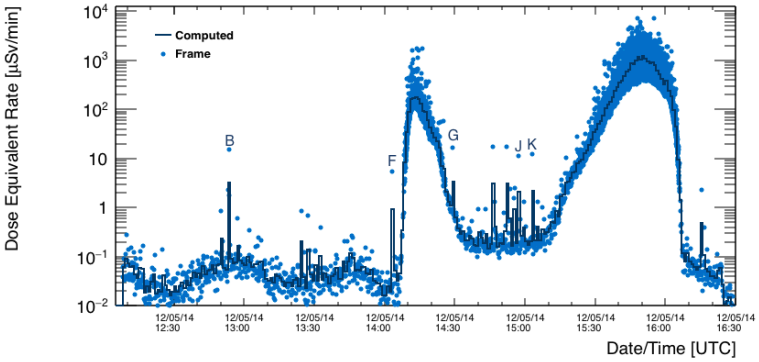

(b) Dose equivalent rate for the right detector, tagged for frames shown below.

Figure 27: Dose equivalent rate in the BIRD, with tags to specific frames shown below.

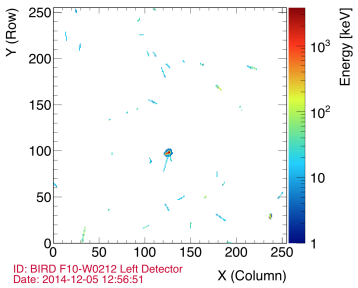

(a) Left detector frame corresponding to tag A in Figure 27.

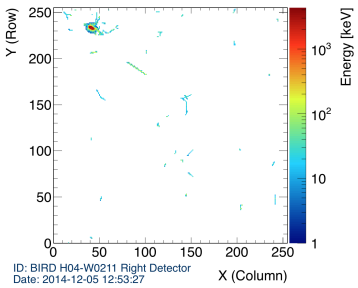

(b) Right detector frame corresponding to tag B in Figure 27.

Figure 28: Example frames from the BIRD prior to the first increase in dose rates.

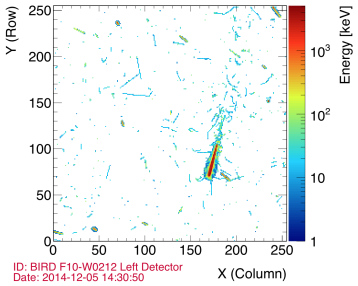

(a) Left detector frame corresponding to tag C in Figure 27.

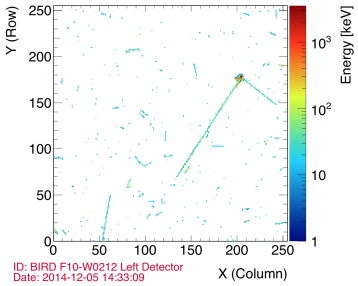

(b) Left detector frame corresponding to tag D in Figure 27.

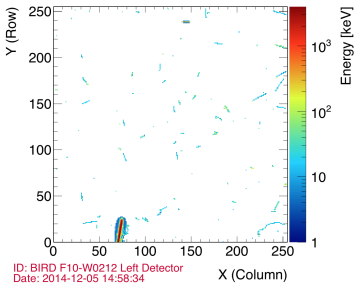

(c) Left detector frame corresponding to tag E in Figure 27.

Figure 29: Example frames from the left detector during the first increase in dose rates.

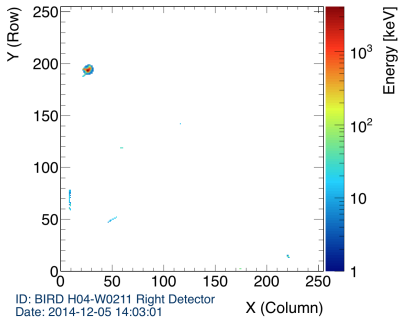

(a) Right detector frame corresponding to tag F in Figure 27.

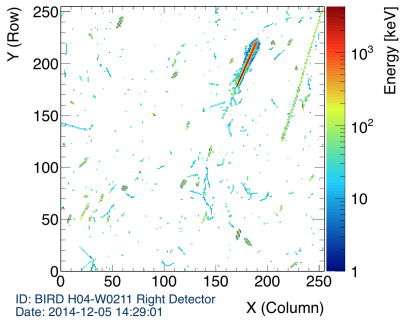

(b) Right detector frame corresponding to tag G in Figure 27.

Figure 30: Example frames from the right detector during first increase in dose rates.

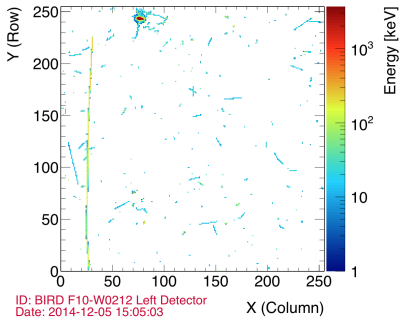

(a) Left detector frame corresponding to tag H in Figure 27.

Figure 31: Example frames from the left detector prior to the second increase in dose rates.

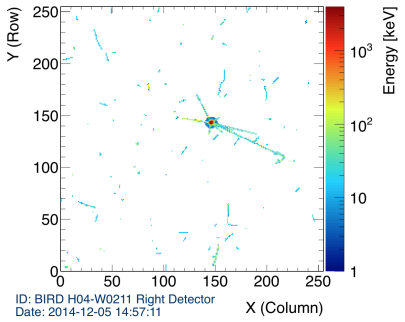

(a) Right detector frame corresponding to tag J in Figure 27.

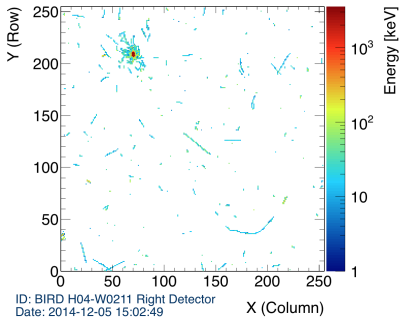

(b) Right detector frame corresponding to tag K in Figure 27.

Figure 32: Example frames from the right detector between the two peaks in dose rates.

5 Summary

The EFT-1 mission presented the first opportunity to take radiation measurements on the Orion MPCV. The BIRD acquired radiation data that are vital for understanding the impacts of transient trapped belt radiation exposures on crew health and safety for future crewed exploration missions. Valuable experience was gained with designing space radiation detection systems around the Timepix technology. This experience is already being put to use in the design of the HERA, which will be the operational radiation monitoring system for the Orion MPCV.

5.1 Detector Operation

The BIRD operated as expected throughout the EFT-1 mission. BIRD was tested and placed in sleep mode prior to integration in the Orion MPCV. After launch, it successfully triggered by sampling the acceleration environment and shut down as anticipated when the battery pack voltage reached a critical level. Temperature data indicate that the thermal environment remained within operational bounds. Radiation data were collected and stored on the BIRD SD cards, and no data corruption was encountered.

5.2 Data

The BIRD data provided a preview of the radiation environment that the crew will encounter while transiting the trapped radiation belts on future exploration missions. Prior to entering the trapped belts, the undulation of the GCR as a result of the varying intensity of Earth's geomagnetic field is observed in Figure 12. Upon entering the trapped belts, a region of high absorbed dose rates was encountered, followed by a local minimum, caused by a softening of the trapped proton energy spectrum. The second region of high absorbed dose rates occurred just after the maximum altitude was reached. The maximum absorbed dose rate was found to be about 1 mGy/min, 20 times the alarm level for the ISS-TEPC.

It is important to note that while these absorbed dose rates are very high, the exposure is transient. For nearly 4.5 hours of mission time, the total absorbed dose to the detectors was less than 20 mGy (water). The results for the BIRD detectors compare favorably with the RAM results, as shown in Table 1. Differences on the order of 10%-15% for co-located RAM and ISS-TEPC detectors are common on the ISS. It is also interesting to note that the cumulative absorbed dose as measured by the ISS-TEPC during the EFT-1 mission was about three orders of magnitude, or 1000 times, less than the cumulative absorbed doses measured on the Orion MPCV.

5.3 Model Comparisons

Intitial comparisons with the AP9/AE9 trapped belt models were performed, assuming an aluminum shield of constant thickness and omnidirectional flux

(Figure 14). Even using these simplifying assumptions, good qualitative agreement is observed between the model and measurements. Future work will focus on characterizing the vehicular shielding around each detector and utilizing the as-flown trajectory to understand the absolute orientation of the BIRD. The angular data presented in Section 4.7 are unique to Timepix-based radiation detection systems and are valuable for comparing theoretical predictions of trapped proton angular distributions with measurements. Additionally, deconvolution of the overlapping tracks will result in a more complete analysis and permit in-depth model comparisons for the highest intensity region of the radiation environment for the EFT-1 mission.

6 References

1. NCRP: Radiation protection guidance for activities in low-Earth orbit. *NCRP Report No. 132*, 2000.

2. NCRP: Information needed to make radiation protection recommendations for space missions beyond low-Earth orbit. *NCRP Report No. 153*, 2006.

3. Llopart, X.; Campbell, M.; Dinapoli, R.; San Segundo, D.; and Pernigotti, E.: Medipix2: a 64-k Pixel Readout Chip With 55-mm Square Elements Working in Single Photon Counting Mode. *IEEE Trans. Nucl. Sci.*, vol. 49, no. 5, 2002, pp. 2361–2365.

4. Llopart, X.; Ballabriga, R.; Campbell, M.; Tlustos, L.; and Wong, W.: Timepix, a 65k Programmable Pixel Readout Chip for Arrival Time, Energy and/or Photon Counting Measurements. *Nuclear Instruments and Methods in Physics Research Section A: Accelerators, Spectrometers, Detectors and Associated Equipment*, vol. 581, no. 1, 2007, pp. 485–494.

5. Campbell, M.: 10 years of the Medipix2 Collaboration. *Nuclear Inst. and Methods in Physics Research A*, vol. 633, 2010, pp. S1–S10.

6. Holy, T.; Jakubek, J.; Pospisil, S.; Uher, J.; Vavrik, D.; and Vykydal, Z.: Data acquisition and processing software package for Medipix2. *Nuclear Inst. and Methods in Physics Research A*, vol. 563, 2006, pp. 254–258.

7. Campbell, M.; Havranek, V.; Heijne, E.; Holy, T.; Idarraga, J.; Jakubek, J.; Lebel, C.; Leroy, C.; Llopart, X.; Novotny, J.; Pospisil, S.; Tlustos, L.; and Vykydal, Z.: Charge collection from proton and alpha particle tracks in silicon pixel detector devices. *Nuclear Science Symposium Conference Record, 2007. NSS'07. IEEE*, IEEE, vol. 2, 2007, pp. 1047–1050.

8. Holy, T.; Heijne, E.; Jakubek, J.; Pospisil, S.; Uher, J.; and Vykydal, Z.: Pattern recognition of tracks induced by individual quanta of ionizing radiation in Medipix2 silicon detector. *Nuclear Inst. and Methods in Physics Research A*, vol. 591, 2008, pp. 287–290.

9. Jakubek, J.; Cejnarova, A.; Holy, T.; Pospisil, S.; Uher, J.; and Vykydal, Z.: Pixel detectors for imaging with heavy charged particles. *Nuclear Inst. and Methods in Physics Research A*, vol. 591, no. 1, 2008, pp. 155–158.

10. Vilalta, R.; Kuchibholta, S.; Valerio, R.; and Pinsky, L.: Development of Pattern Recognition Software for Tracks of Ionizing Radiation in Medipix2-Based (Timepix) Pixel Detector Devices. *J. of Physics:Conf. Series*, vol. 331, 2011, pp. 32052–32058.

11. Hoang, S.; Pinsky, L.; Vilalta, R.; and Jakubek, J.: LET Estimation of Heavy Ion Particles based on a Timepix-Based Si Detector. *Journal of Physics: Conference Series*, vol. 396, no. 2, 2012, p. 022023.

12. Hoang, S.; Vilalta, R.; Pinsky, L.; Kroupa, M.; Stoffle, N.; and Idarraga, J.: Data Analysis of Tracks for Heavy Ion Particles in Timepix Detectors. *J. of Physics:Conf. Series*, vol. 523, 2014, pp. 12026–12034.

13. International Space Exploration Coordination Group (ISECG): The Global Exploration Roadmap. NP-2013-06-945-HQ, International Space Exploration Coordination Group (ISECG), August 2013. URL `http://www.nasa.gov/sites/default/files/files/GER-2013_Small.pdf`, accessed: 2015-02-09.

14. NASA: Voyages: Charting the Course for Sustainable Human Space Exploration. NP-2011-06-395-LaRC, NASA, June 2012. URL `http://www.nasa.gov/sites/default/files/files/ExplorationReport_508_6-4-12.pdf`, accessed: 2015-02-09.

15. Stoffle, N.; Pinsky, L.; Kroupa, M.; Hoang, S.; Idarraga, J.; Amberboy, C.; Rios, R.; Hauss, J.; Bahadori, A.; Semones, E.; Turecek, D.; Jakubek, J.; Vykydal, Z.; and Pospisil, S.: Timepix-based Radiation Environment Monitor Measurements Aboard the International Space Station. *Nuclear Instruments and Methods in Physics Research Section A: Accelerators, Spectrometers, Detectors and Associated Equipment*, vol. 782, 2015, pp. 143–148.

16. NASA: Journey to Mars. URL `http://www.nasa.gov/sites/default/files/thumbnails/image/journey_to_mars.jpeg`, accessed: 2015-02-09.

17. NASA: Orion First Test Flight NASAfacts. FS-2014-08-005-JSC, NASA, 2014. URL `http://www.nasa.gov/sites/default/files/fs-2014-08-005-jsc-orion-eft-final.pdf`, accessed: 2015-02-09.

18. NASA: Orion Exploration Flight Test-1 NASAfacts. FS-2012-05-018-JSC, NASA, 2012. URL `http://www.nasa.gov/pdf/663703main_flighttest1_fs_051812.pdf`, accessed: 2015-02-09.

19. AES Radworks REM: Concept of Operations Document for the BIRD on EFT-1, Revision A. RDWK-10101, NASA, 2014.

20. AES RadWorks REM: Verification and Validation Document: Plan and Report for the BIRD. RDWK-10096, NASA, 2013.

21. Memorandum for Record. SA-13-070, NASA, 2013.

22. Gaza, R.; Zhou, D.; Roed, Y.; Semones, E.; and Zapp, N.: Summary of 2008-2009 SRAG's Radiation Measurements in Low-Earth Orbit using Passive Radiation Detectors, 2009. URL `http://wrmiss.org/workshops/fourteenth/`, fourteenth Annual Workshop on Radiation Monitoring for the International Space Station - Dublin, Ireland.

23. Gaza, R.; Bahadori, A.; Fry, D.; Lee, K.; and Semones, E.: ISS Radiation Area Monitors Measurements at Solar Maximum, 2013. URL `http://wrmiss.org/workshops/eighteenth/Gaza.pdf`, eighteenth Annual Workshop on Radiation Monitoring for the International Space Station - Budapest, Hungary.

24. Gaza, R.; Welton, A.; Dunegan, A.; Fry, D.; and Lee, K.: ISS and Space Shuttle Radiation Measurements at Solar Minimum, 2011. URL `http://wrmiss.org/workshops/sixteenth/`, sixteenth Annual Workshop on Radiation Monitoring for the International Space Station - Prague, Czech Republic.

25. Reitz, G.; Berger, T.; Bilski, P.; Facius, R.; Hajek, M.; Petrov, V.; Puchalska, M.; Zhou, D.; Bossler, J.; Akatov, Y.; Shurshakov, V.; Olko, P.; Ptaszkiewicz, M.; Bergmann, R.; Fugger, M.; Vana, N.; Beaujean, R.; Burmeister, S.; Bartlett, D.; Hager, L.; Pálfalvi, J.; Szabó, J.; O'Sullivan, D.; Kitamura, H.; Uchihori, Y.; Yasuda, N.; Nagamatsu, A.; Tawara, H.; Benton, E.; Gaza, R.; McKeever, S.; Sawakuchi, G.; Yukihara, E.; Cucinotta, F.; Semones, E.; Zapp, N.; Miller, J.; and Dettman, J.: Astronaut's organ dose as inferred from measurements using a human phantom outside the ISS. *Radiation Research*, vol. 171, 2009, pp. 225–235.

26. McKeever, S. W. S.; Gaza, R.; and Yukihara, E. G.: TL and OSL efficiencies of Al_2O_3:C and LiF:Mg,Ti detectors exposed during ICCHIBAN-2. HIMAC-078, National Institute of Radiological Sciences, 2004.

27. Gaza, R.; Yukihara, E. G.; and McKeever, S. W. S.: The response of thermally and optically stimulated luminescene from Al_2O_3:C to high-energy heavy charged particles. *Radiation Measurements*, vol. 38, 2004, pp. 417–420.

28. Brun, R.; and Rademakers, F.: ROOT - An Object Oriented Data Analysis Framework. *Nuclear Instruments and Methods in Physics Research Section A: Accelerators, Spectrometers, Detectors and Associated Equipment*, vol. 389, no. 1-2, Apr 1997, pp. 81–86. See also http://root.cern.ch/.

29. Jakubek, J.: Precise Energy Calibration of Pixel Detector Working in Time-Over-Threshold Mode. *Nuclear Instruments and Methods in Physics Research Section A: Accelerators, Spectrometers, Detectors and Associated Equipment*, vol. 633, 2011, pp. S262–S266.

30. ICRP: 1990 Recommendations of the International Commission on Radiological Protection. ICRP Publication 60. *Ann. ICRP*, vol. 21, no. 1-3, 1991.

31. Energizer Battery Manufacturing Inc.: *Energizer Lithium Iron Disulfide Handbook and Application Manual*. Li4.04 ed., 2013. `http://data.energizer.com/PDFs/lithiuml91l92_appman.pdf`.

32. Ginet, G.; O'Brien, T.; Huston, S.; Johnston, W.; Guild, T.; Friedel, R.; Lindstrom, C.; Roth, C.; Whelan, P.; Quinn, R.; Madden, D.; Morley, S.; and Su, Y.-J.: AE9, AP9 and SPM: New Models for Specifying the Trapped Energetic Particle and Space Plasma Environment. *Space Science Reviews*, vol. 179, no. 1-4, 2013, pp. 579–615. URL `http://dx.doi.org/10.1007/s11214-013-9964-y`.

33. Web., February 2015. URL `https://www.google.com/earth/`.

34. Benton, E.; and Benton, E.: Space radiation dosimetry in low-Earth orbit and beyond. *Nuclear Instruments and Methods in Physics Research Section B: Beam Interactions with Materials and Atoms*, vol. 184, no. 1-2, 2001, pp. 255 – 294. Advanced Topics in Solid State Dosimetry.

REPORT DOCUMENTATION PAGE

Form Approved
OMB No. 0704–0188

The public reporting burden for this collection of information is estimated to average 1 hour per response, including the time for reviewing instructions, searching existing data sources, gathering and maintaining the data needed, and completing and reviewing the collection of information. Send comments regarding this burden estimate or any other aspect of this collection of information, including suggestions for reducing this burden, to Department of Defense, Washington Headquarters Services, Directorate for Information Operations and Reports (0704-0188), 1215 Jefferson Davis Highway, Suite 1204, Arlington, VA 22202-4302. Respondents should be aware that notwithstanding any other provision of law, no person shall be subject to any penalty for failing to comply with a collection of information if it does not display a currently valid OMB control number.
PLEASE DO NOT RETURN YOUR FORM TO THE ABOVE ADDRESS.

1. REPORT DATE *(DD-MM-YYYY)*	2. REPORT TYPE	3. DATES COVERED *(From - To)*
01-06-2015	Technical Publication	

4. TITLE AND SUBTITLE
Battery-operated Independent Radiation Detector Data Report from Exploration Flight Test 1

5a. CONTRACT NUMBER

5b. GRANT NUMBER

5c. PROGRAM ELEMENT NUMBER

6. AUTHOR(S)
Amir A. Bahadori, Edward J. Semones, Ramona Gaza, Martin Kroupa, Ryan R. Rios, Nicholas N. Stoffle, Thomas Campbell-Ricketts, Lawrence S. Pinsky, Daniel Turecek

5d. PROJECT NUMBER

5e. TASK NUMBER

5f. WORK UNIT NUMBER

7. PERFORMING ORGANIZATION NAME(S) AND ADDRESS(ES)
NASA Johnson Space Center
Houston, Texas 77058

8. PERFORMING ORGANIZATION REPORT NUMBER
SRAG-INT-BIRD-2015-001

9. SPONSORING/MONITORING AGENCY NAME(S) AND ADDRESS(ES)
National Aeronautics and Space Administration
Washington, DC 20546-0001

10. SPONSOR/MONITOR'S ACRONYM(S)
NASA

11. SPONSOR/MONITOR'S REPORT NUMBER(S)
NASA/TP–2015–218575

12. DISTRIBUTION/AVAILABILITY STATEMENT
Unclassified-Unlimited
Subject Category 93
Availability: NASA CASI (443) 757-5802

13. SUPPLEMENTARY NOTES
An electronic version can be found at http://ntrs.nasa.gov.
An errata was added to this document, October 2016.

14. ABSTRACT
This report summarizes the data acquired by the Battery-operated Independent Radiation Detector (BIRD) during Exploration Flight Test 1 (EFT-1). The BIRD, consisting of two redundant subsystems isolated electronically from the Orion Multi-Purpose Crew Vehicle (MPCV), was developed to fly on the Orion EFT-1 to acquire radiation data throughout the mission. The BIRD subsystems successfully triggered using on-board accelerometers in response to launch accelerations, acquired and archived data through landing, and completed the shut down routine when battery voltage decreased to a specified value. The data acquired are important for understanding the radiation environment within the Orion MPCV during transit through the trapped radiation belts.

15. SUBJECT TERMS
Orion, MPCV, EFT1, BIRD, Radiation

16. SECURITY CLASSIFICATION OF:			17. LIMITATION OF ABSTRACT	18. NUMBER OF PAGES	19a. NAME OF RESPONSIBLE PERSON
a. REPORT	b. ABSTRACT	c. THIS PAGE			STI Information Desk (help@sti.nasa.gov)
U	U	U	UU	54	19b. TELEPHONE NUMBER *(Include area code)* (443) 757-5802